ACS ES&T Water

pubs.acs.org/estwater

Article

Ferrate(VI) Oxidation of Pharmaceuticals in Hydrolyzed Urine: Enhancement by Creatinine and the Role of Fe(IV)

Cong Luo, Mingbao Feng, Tianqi Zhang, Virender K. Sharma,* and Ching-Hua Huang*

Cite This: *ACS EST Water* 2021, 1, 969–979

Read Online

ACCESS | Metrics & More | Article Recommendations | Supporting Information

ABSTRACT: Treatment of human urine is an emerging approach to minimize environmental pharmaceutical contamination. This study investigated the application of ferrate(VI) ($Fe^{VI}O_4^{2-}$, Fe(VI)) oxidation to degrade pharmaceuticals (i.e., carbamazepine (CBZ), naproxen (NAP), sulfamethoxazole (SMX), and trimethoprim (TMP)) in synthetic hydrolyzed human urine, with the emphasis on the effects of urine endogenous organic metabolites. Creatine and hippuric acid showed limited to moderate scavenging effects. Creatinine (CRE) was first discovered to significantly enhance the oxidation rates of CBZ, TMP, SMX, and other amine-containing compounds by Fe(VI). Fe(IV) was proposed as the major intermediate reactive iron species in the Fe(VI)−CRE system, based on the DFT calculation and experimental measurements. A kinetic model involving Fe(IV) contribution in the decay of the pharmaceuticals was developed for the first time to successfully describe the pharmaceutical removal in the Fe(VI)−CRE−micropollutant system. Moreover, the model was used to predict the rate constants of Fe(IV) reacting with different compounds, which ranged from $(2.2 \pm 0.1) \times 10^4$ to $(8.3 \pm 0.6) \times 10^4$ M^{-1} s^{-1}. Overall, this study further demonstrated the promise of Fe(VI) oxidation to degrade pharmaceuticals in hydrolyzed urine owing to the enhanced effects from urine constituents. This study also advanced the mechanistic and kinetic understanding of enhanced oxidation involving high-valent iron intermediate species.

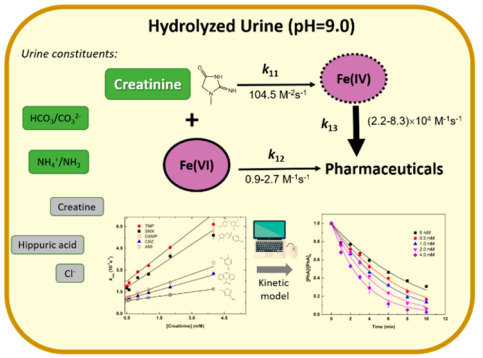

KEYWORDS: *ferrate, Fe(VI), Fe(IV), urine treatment, creatinine*

INTRODUCTION

Among all the wastewater streams that are directed into wastewater treatment plants, human urine has been regarded as a minuscule yet critical component, that is, at only 0.6% by volume but contributing to more than 64% of pharmaceuticals, 80% of nitrogen, and 50% of phosphorus on a mass basis.[1,2] Thus, the treatment of source-separated urine has emerged as a disruptive innovation to the status quo approach to wastewater management because it can be efficient in recovering nutrients into usable fertilizers and destructing pharmaceutical micropollutants.

To date, research regarding the removal of pharmaceuticals and their metabolites in urine is still limited. Nanofiltration membranes,[3] strong-base anion exchange resins,[4] electrodialysis,[5] struvite precipitation,[6] and biochar[7] have been investigated previously. All of the above methods, however, only physically separate pharmaceuticals from urine and generate pharmaceutical wastes that still need to be treated. Ozonation,[8] UV/H_2O_2, and UV/pexroxydisulfate (PDS)[9] were investigated for destruction of pharmaceuticals in urine; however, the efficiency of these treatment processes was significantly decreased by the strong scavenging effects of the urine constituents, particularly from the high concentrations of ammonium, bicarbonate, and chloride. In contrast, our recent study unveiled the use of ferrate(VI) ($Fe^{VI}O_4^{2-}$, Fe(VI)) for oxidizing pharmaceuticals in hydrolyzed urine, and observed that inorganic constituents (e.g., ammonium and bicarbonate) could enhance the degradation of pharmaceuticals by Fe(VI).[10] However, the potential effects of common organic metabolites in urine on the Fe(VI) oxidation of pharmaceuticals still remained unknown and required additional investigation. In general, the occurrence of organic metabolites in human urine has not been taken into account in the synthetic urine recipes employed in many previous studies, and, as a result, the influence of common organic metabolites on the oxidative removal of pharmaceuticals in urine has been neglected or poorly understood.

Data on endogenous metabolites in human urine are mostly from the medical literature and are almost exclusively for fresh urine. More than 2651 human urine metabolites have been identified,[11] with creatinine (CRE), creatine, hippuric acid,

Received: November 18, 2020
Revised: December 28, 2020
Accepted: January 6, 2021
Published: January 12, 2021

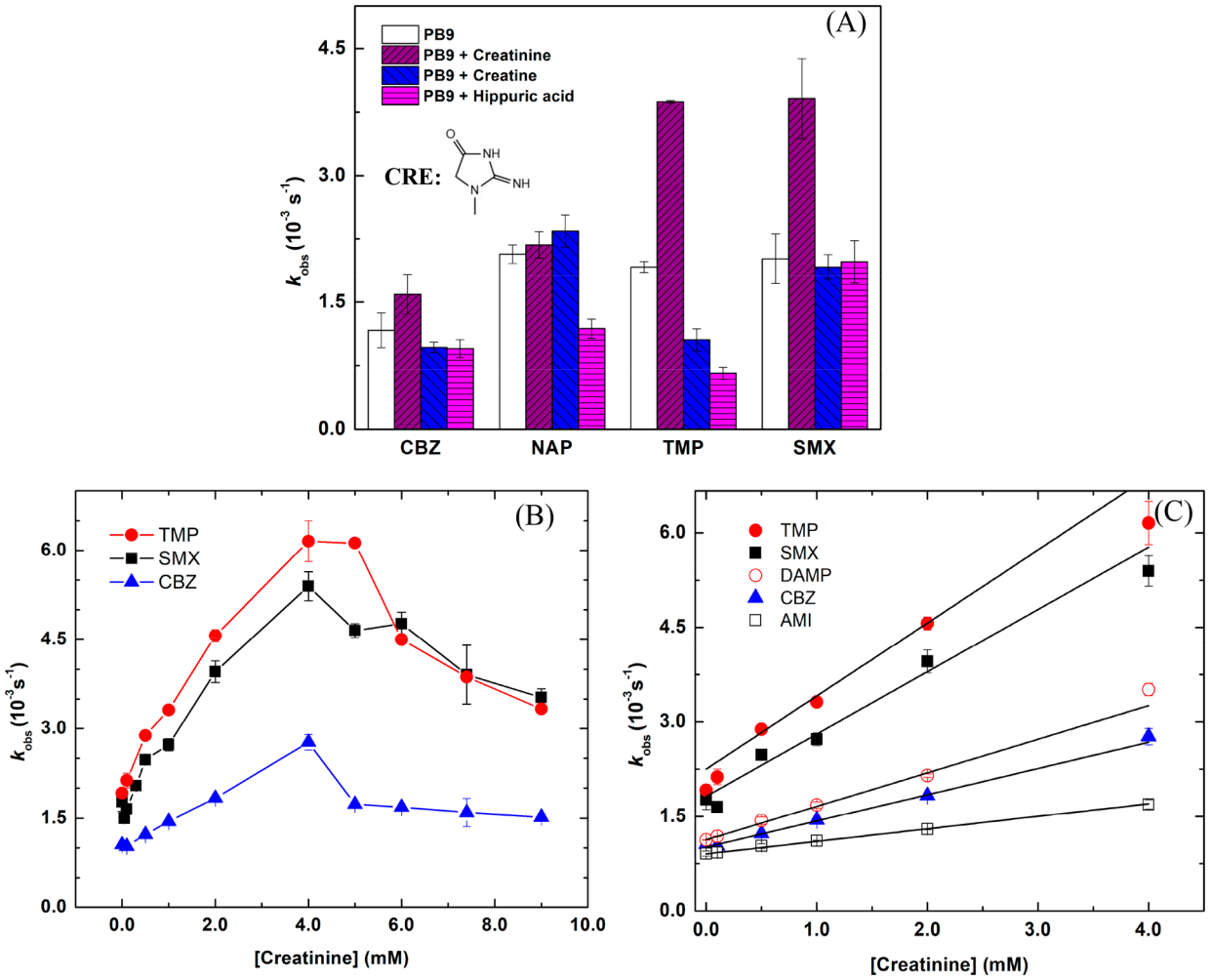

Figure 1. (A) Effect of organic metabolites on Fe(VI) oxidation of pharmaceuticals. Initially, [micropollutant] = 10.0 μM, [Fe(VI)] = 300.0 μM, [CRE] = 7.4 mM, [creatine] = 1.28 mM, [hippuric acid] = 0.17 mM. (B) Effect of CRE on Fe(VI) oxidation of pharmaceuticals. Initially, [micropollutant] = 10.0 μM, [Fe(VI)] = 300.0 μM, [CRE] = 0–9.0 mM. (C) Effect of CRE on Fe(VI) oxidation of pharmaceuticals and their substructure compounds. Initially, [micropollutant] = 10.0 μM, [Fe(VI)] = 300.0 μM, [CRE] = 0–4.0 mM, and R^2 = 0.982–0.999. All reactions were at pH 9.0 (10.0 mM phosphate buffer), 25.0 °C, and n = 2.

citric acid, glycine, taurine, and L-cysteine being the most prevalent and at the highest concentrations (1–15 mM).[11] CRE is typically measured during standard urine drug testing due to its relatively stable chemistry and ubiquitous concentrations. A decrease in chemical oxygen demand (COD) was reported in stored urine upon the transformation of fresh urine to hydrolyzed urine, suggesting that endogenous metabolites were degraded to some extent during aging of urine.[12] Even so, CRE, creatine, and hippuric acid were still among the most concentrated organic metabolites found in hydrolyzed urine.[13,14] Therefore, these three compounds were selected in this study to represent the common endogenous metabolites in urine.

As shown in Supporting Information (SI) Table S1, CRE is a cyclic amino acid with a five-membered ring, a guanidine group and a peptide bond, creatine is a linear amino acid, and hippuric acid is the glycine conjugate of benzoic acid. The sources, distribution and typical concentration ranges of CRE, creatine and hippuric acid in human urine are detailed in SI Text S1. Taking into account the typical concentration ranges of these organic metabolites in fresh human urine and the potential degradation that could occur during the transformation of fresh urine to hydrolyzed urine, the concentrations of 7.4 mM CRE, 1.28 mM creatine, and 0.17 mM hippuric acid were considered representative for hydrolyzed urine in this study.

While many studies have investigated removal of contaminants from water by Fe(VI),[15,16] only limited efforts were dedicated to understanding the mechanisms of Fe(VI) oxidation reactions involving high-valent iron intermediate species, that is, Fe(V)/Fe(IV). In recent years, there has been increasing attention on the enhanced role of Fe(V)/Fe(IV) during Fe(VI) oxidation in the presence of inorganic activators such as ammonia,[17] acid,[18] sulfite/thiosulfate,[19] bicarbonate,[10] Fe(II)/Fe(III),[20] and Mn(II).[21] However, previous research mainly relied on qualitative analysis of possible reactive species generated (radical vs Fe(V)/Fe(IV)), and the kinetic behaviors (self-decay vs oxidation of micropollutants) of Fe(V)/Fe(IV) in the oxidation process remained unclear. As will be shown later, urine CRE can act as an "activator" to generate high-valent iron intermediate species.

Therefore, the objective of this work was to assess the efficacy of Fe(VI) to degrade pharmaceuticals in synthetic hydrolyzed urine matrix with naturally existing organic

https://dx.doi.org/10.1021/acsestwater.0c00255
ACS EST Water 2021, 1, 969–979

metabolites and to fully elucidate the kinetic behaviors of high-valent iron intermediate species (i.e., Fe(V)/Fe(IV)) during Fe(VI) oxidation in the presence of CRE. Four pharmaceuticals (i.e., carbamazepine (CBZ), naproxen (NAP), trimethoprim (TMP), and sulfamethoxazole (SMX)) that are frequently detected in the environment[22,23] were selected as the representative micropollutants. Experiments were conducted using synthetic hydrolyzed urine (SHU)[14,24] with modifications or buffered solutions to delineate the specific effects of CRE, creatine, and hippuric acid. To the best of our knowledge, the finding of the organic activator—CRE—in the Fe(VI) oxidation is among the first. Additionally, this paper fully examined the role of Fe(IV) species in the Fe(VI)−CRE−micropollutant system by new kinetic model simulation and predicted the rate constants between Fe(IV) species and several micropollutants.

MATERIALS AND METHODS

Chemicals. Sources of chemicals and reagents are provided in the SI Text S2. Structures and chemical properties of the target pharmaceuticals are shown in SI Table S1.

Reaction Matrices. SHU was prepared similarly to the previous studies[10,25] and the composition is listed in SI Table S2. Briefly, SHU contained 0.50 M total ammonia (NH_3 + NH_4^+), 0.25 M total carbonate (HCO_3^- + CO_3^{2-}), 0.10 M chloride, 7.40 mM CRE, 1.28 mM creatine, 0.17 mM hippuric acid, as well as Na^+, K^+, SO_4^{2-} and phosphate. Solution pH was adjusted to 9.0 using the concentrated solutions of NaOH and NaH_2PO_4. To evaluate the effect of individual urine constituents, phosphate buffer (10.0 mM) solution at pH 9.0 (PB9) was spiked with specific urine constituent at various concentrations and compared with the PB9 control matrix without urine constituents. The phosphate buffer concentration was comparable to that in SHU and commonly used in ferrate research.

Oxidation Experiments and Analysis. The procedures of Fe(VI) oxidation of different pharmaceuticals at different reaction matrices followed those described in our recent study.[10] Briefly, PB9 and modified PB9 (50.0 mL) were first spiked with the target pharmaceutical (10.0 μM). Then, 2.97 mg of potassium ferrate(VI) was weighed and added immediately to the reaction solution (achieving 300.0 μM) to initiate the oxidation process. Sample aliquots were taken from the reaction solution at predetermined time intervals and quenched immediately by sodium thiosulfate (2.5 mM).[38] Solution pH was checked before and after the reaction by a pH meter (Accumet Research AR 20) and change was never larger than 0.2 pH unit. Degradation of micropollutants and generation of methyl phenyl sulfone ($PMSO_2$) were monitored by high performance liquid chromatography (HPLC)-diode array detection (DAD), and the transformation products of SMX by Fe(VI) were analyzed using solid-phase extraction (SPE) followed by HPLC-high resolution mass spectrometry (LC-HRMS) analysis. Detailed analytical methods are described in SI Text S3.

Computations and Kinetic Modeling. The density functional theory (DFT) calculations for reaction energies are described in SI Text S4. The kinetic modeling was conducted via the least-squares nonlinear regression with constant error model by using SimBiology version 5.7 in MATLAB 2018 (The Math Works, Inc.). The goodness-of-fit between simulated and experimental values was quantified by calculating the Theil's inequality coefficient (TIC),[26] the normalized root-mean-square error (NRMSE), and the model efficiency (ME).[27]

RESULTS AND DISCUSSION

Impacts of Organic Metabolites on Pharmaceutical Degradation by Fe(VI). Experiments using PB9 spiked with CRE, creatine or hippuric acid individually were conducted to evaluate their effects on the Fe(VI) oxidation of pharmaceuticals. As shown by the pseudo-first-order rate constants (k_{obs} in s^{-1}, $R^2 > 0.985$) in Figure 1A, CRE significantly enhanced the degradation of pharmaceuticals by Fe(VI), especially for the cases of CBZ, TMP, and SMX, whereas creatine and hippuric acid had limited to moderate impacts on the removal efficiency of the four pharmaceuticals by Fe(VI).

To better understand the enhanced effect of CRE on the oxidation of pharmaceuticals by Fe(VI), the impact of CRE concentration on the removal of pharmaceuticals by Fe(VI) was investigated for CBZ, TMP, and SMX. The k_{obs} increased linearly as the CRE concentration was increased from 0 to 4.0 mM (Figure 1B) but then decreased when the CRE concentration was above 4.0 mM and up to 9.0 mM for all three pharmaceuticals. The decrease of enhanced degradation rates of pharmaceuticals observed at above 4.0 mM of CRE could be due to additional reactions created under a high dosage of CRE that affected intermediate iron species (see more discussion later).

Elucidating the Enhanced Effect of CRE. *Reactive Moiety.* To determine the likely initial attack position(s) on the pharmaceuticals by Fe(VI) in the presence of CRE, the substructure compounds of TMP (i.e., 2,4-diamino-5-methylpyrimidine (DAMP) and 3,4,5-trimethoxytoluene (TMT)) and SMX (i.e., 3-amino-5-methylisoxazole (AMI), 3,5-dimethylisoxazole (DMI), and aniline) were investigated for their reactions with Fe(VI) in the presence and absence of CRE at pH 9.0. For the subunits of TMP, degradation of TMT by Fe(VI) was negligible (SI Figure S1A), which was also confirmed by a previous study.[28] Even in the presence of CRE (0−0.5 mM), there was no noticeable degradation of TMT observed in the Fe(VI)−CRE system. On the other hand, DAMP, the subunit containing the amine group in TMP, showed the enhanced effect from CRE as seen in Figure 1C, where k_{obs} increased 3.1 times when CRE concentration was increased from 0 to 4.0 mM. For the subunits of SMX, degradation of DMI by Fe(VI) was inhibited by the presence of CRE, where k_{obs} decreased from 4.6×10^{-2} to 2.9×10^{-2} min^{-1} when CRE concentration was increased from 0 to 4.0 mM (SI Figure S1B), while AMI, with its amine group substituting the methyl group in DMI, showed a strong positive linear relationship between k_{obs} and CRE concentration (Figure 1C). This amine-structure-specific effect from CRE could be further confirmed by Fe(VI) oxidation of aniline, a subunit of SMX, in the presence of CRE. As SI Figure S1C shows, the k_{obs} of degradation of aniline by Fe(VI) increased 3.7 times when CRE concentration was increased from 0 to 0.5 mM.

Role of Radical Species. Several studies[29−32] have found that imidazole and CRE, when complexed with specific metal ions (e.g., Cu^{2+} and Fe^{3+}), can display peroxidase activity to activate H_2O_2 and generate hydroxyl radical ($^{\cdot}OH$). It is also interesting to note that Fe(III) and H_2O_2 are considered two major products generated from the self-decay of Fe(VI), as well as the reaction of Fe(VI) with organic substrates.[33] Therefore, it is reasonable to hypothesize that CRE, when

https://dx.doi.org/10.1021/acsestwater.0c00255
ACS EST Water 2021, 1, 969−979

complexed with Fe(III) produced from Fe(VI) reduction, may show catalytic activity to promote the generation of highly reactive ·OH from H_2O_2, which can also be produced from Fe(VI) reduction. *Para*-chlorobenzoic acid (*p*CBA) was chosen as the quencher for ·OH for its inert reactivity to high-valent iron species (Fe(VI)/Fe(V)[34] and Fe(IV)[35]) and high reactivity to ·OH with a second-order rate constant of 5×10^9 M^{-1} s^{-1} at pH 8.[36] As Figure 2A shows, the degradation trends of SMX were similar in the presence or absence of *p*CBA. Therefore, the results ruled out the possible generation of ·OH in the Fe(VI)−CRE system.

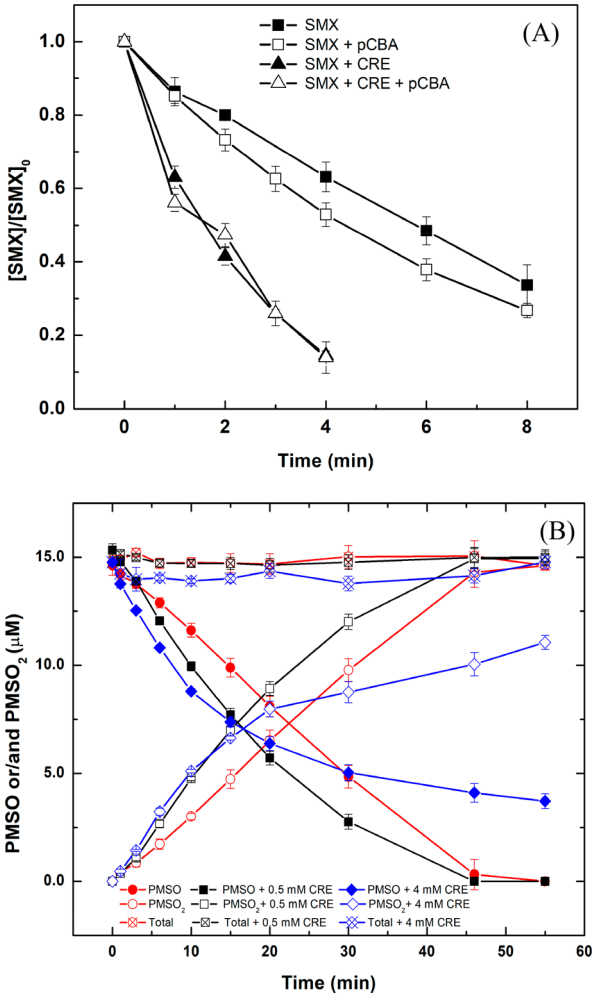

Figure 2. (A) Effect of *p*CBA on Fe(VI) oxidation of SMX in the presence or absence of CRE. Initially, [SMX] = 10.0 μM, [Fe(VI)] = 500.0 μM, [CRE] = 7.4 mM, [*p*CBA] = 100.0 μM. (B) PMSO oxidation and $PMSO_2$ production in the Fe(VI)−CRE system. Initially, [PMSO] = 15.0 M, [Fe(VI)] = 300.0 μM, [CRE] = 0−4.0 mM. All reactions were at pH 9.0 (10.0 mM phosphate buffer), 25 °C, and n = 2.

Role of Iron Intermediate Species. High-valent iron species (e.g., Fe(IV),[37−39] Fe(V),[40] and Fe(VI)[41]) were reported to be reactive with sulfoxide (e.g., dimethyl sulfoxide (DMSO) and methyl phenyl sulfoxide (PMSO)), generating corresponding sulfones (e.g., dimethyl sulfone ($DMSO_2$) and methyl phenyl sulfone ($PMSO_2$)) via an oxygen atom transfer (OAT) step under both acidic and alkaline conditions. This reaction pathway differs dramatically from the radical-based oxidation pathway, which normally turns DMSO or PMSO into their ·OH-induced products (e.g., CH_3SO_2H).[38] Thus, PMSO was used as the probe compound to investigate the involvement of high-valent iron intermediate species.

As Figure 2B shows, PMSO was completely oxidized to $PMSO_2$ by Fe(VI) in the presence of 0−4.0 mM CRE, which further eliminated the possibility of radical involvement in the Fe(VI)−CRE system and agreed with the above results based on radical quencher (i.e., *p*CBA) experiments. In the presence of CRE, PMSO degradation, and $PMSO_2$ generation were accelerated with an increased concentration of CRE, especially within the first 15 min, which further verified that Fe(V) and/or Fe(IV) were likely responsible for the enhanced rates observed in the Fe(VI)−CRE system based on the superior oxidation capability of Fe(V)[42] /Fe(IV)[43] to Fe(VI). However, the conversion percentage of PMSO suffered at the higher dosage of CRE (4.0 mM vs 0.5 mM) from 15 to 55 min, which was most likely due to outperformance of the reaction between Fe(V)/Fe(IV) and the oxidized products (OPs) of CRE.

It has been reported that the oxidation of a substrate (X) by Fe(VI) can occur by several possible pathways.[44,45] Steps include but are not limited to (i) 1-e^- transfer to form Fe(V) and a radical, with Fe (V) reacting to form oxidized substrate (X(O)) and Fe(III); (ii) OAT process to produce Fe(IV) and an oxygen atom added to substrate (X(O)); (iii) Fe(V) and Fe(IV) can then yield different final reduced species (i.e., Fe(III) or Fe(II) or both Fe(III) and Fe(II)) via 1-e^- and 2-e^- pathways through self-decomposition and/or further oxidation of substrate (X). Some studies have offered insights on the mechanisms of Steps i and ii, in which the 1-e^- transfer reductants ($R_{(1)}$) or 2-e^- transfer reductants ($R_{(2)}$) were determined through theoretically correlating the reaction rate constants of Fe(VI) with substrates to the 1-e^- or 2-e^- thermodynamic reduction potentials.[46−48]

To further confirm the role of CRE in the Fe(VI)−CRE system as $R_{(1)}$ or $R_{(2)}$, we conducted the low-temperature electron paramagnetic resonance (LT-EPR) measurement with *N*-(4-pyridylmethylene)-*tert*-butylamine-*N*,*N*′-dioxide (POBN) as the spin trap reagent to probe the formation of CRE radical as well as ·OH in the system.[49] This approach has been applied in the Fe(VI)-aniline system, in which the anilino radical was observed during Fe(VI) oxidation of aniline and thus, Fe(V) was speculated as the major reactive iron intermediate species followed by the mechanism of Step i.[50] However, according to SI Figure S2, no obvious signal was detected, indicating that it was less likely that Fe(V) and CRE radical were involved in the Fe(VI)−CRE system. This result also further confirmed the absence of ·OH, which agreed well with the quencher experiment using *p*CBA (Figure 2A). On the other hand, the DFT calculations were performed to examine the favorable step of the reaction between Fe(VI) and CRE to further confirm the role of CRE as $R_{(1)}$ or $R_{(2)}$. Based on the optimized geometries of all species involved (e.g., Fe(VI), Fe(V), Fe(IV), CRE radical, and CRE-O adduct), the changes of Gibbs free energy (ΔG°_{Cal}) and activation energy ($\Delta G^{\ddagger}_{Cal}$) were calculated for reactions R1 (1-e^- transfer) and R2 (2-e^- transfer), respectively. As SI Figure S3 shows, R2 had a negative Gibbs free energy value (ΔG^{0}_{Cal} = −6.37 kJ/mol) with a lower activation energy ($\Delta G^{\ddagger}_{Cal}$ = 3.18 kJ/mol) as compared to R1 (ΔG^{0}_{Cal} = 196.71 kJ/mol and $\Delta G^{\ddagger}_{Cal}$ = 8.66 kJ/mol). This indicated the spontaneity of two-electron transfer reaction and involvement of Fe(IV) as the major reactive oxidant followed in the mechanism of Step ii. This

https://dx.doi.org/10.1021/acsestwater.0c00255
ACS EST Water 2021, 1, 969−979

Table 1. Major Reactions in the Fe(VI)−CRE−Micropollutant System at pH 9.0

reactions	k at pH 9.0	reference
$Fe^{VI}O_4^{2-} + H_2O \rightarrow Fe^{IV}O_3^{2-} + H_2O_2$ (1)	4.8×10^{-5} s^{-1}	55
$Fe^{VI}O_4^{2-} + H_2O_2 \rightarrow Fe^{IV}O_3^{2-} + O_2 + H_2O$ (2)	~ 0 M^{-1} s^{-1}	56
$Fe^{IV}O_3^{2-} + Fe^{IV}O_3^{2-} \rightarrow Fe_2^{IV}O_6^{4-}$ (3)	~ 10^7 M^{-1} s^{-1}	61
$Fe_2^{IV}O_6^{4-} + 4H_2O + 4H^+ \rightarrow 2Fe^{III}(OH)_3(H_2O) + H_2O_2$ (4)	10^2 s^{-1}	61
$Fe^{IV}O_3^{2-} + H_2O_2 + 2H^+ \rightarrow Fe^{II}(OH)_2(aq) + O_2 + H_2O$ (5)	3.0×10^3 M^{-1} s^{-1}	61,68
$Fe^{IV}O_3^{2-} + Fe^{II}(OH)_2(aq) + 3H_2O \rightarrow 2Fe^{III}(OH)_3(aq) + 2OH^-$ (6)	~ 10^6 M^{-1} s^{-1}	61
$Fe^{VI}O_4^{2-} + Fe^{II}(OH)_2(aq) + H_2O \rightarrow HFe^{V}O_4^{2-} + Fe^{III}(OH)_3(aq)$ (7)	~ 10^5 M^{-1} s^{-1}	69,70
$Fe^{II}(OH)_2(aq) + H_2O_2 + 2OH^- \rightarrow Fe^{IV}O_3^{2-} + 3H_2O$ (8)	~ 10^3 M^{-1} s^{-1}	71
$HFe^{V}O_4^{2-} + 2H^+ + 4H_2O \rightarrow Fe^{III}(OH)_3(H_2O)_3 + H_2O_2$ (9a)	5.0 s^{-1}	72
$HFe^{V}O_4^{2-} + HFe^{V}O_4^{2-} + 4H_2O + 4H^+ \rightarrow 2Fe^{III}(OH)_3(H_2O) + 2H_2O_2$ (9b)	1.5×10^7 M^{-1} s^{-1}	73
$HFe^{V}O_4^{2-} + H_2O_2 + H_2O \rightarrow Fe^{III}(OH)_3(aq) + O_2 + 2OH^-$ (10)	4.0×10^5 M^{-1} s^{-1}	56
$2Fe^{VI}O_4^{2-} + CRE \rightarrow 2Fe^{IV}O_3^{2-} + P_1$ (11)	104.5 $M^{-2}s^{-1}$	derived in the Fe(VI)−CRE system
$Fe^{VI}O_4^{2-} + TMP \rightarrow Fe^{III}(OH)_3 + P_1$ (12a)	(2.7 ± 0.4) M^{-1} s^{-1}	estimated in the Fe(VI)−CRE−micropollutant system
$Fe^{VI}O_4^{2-} + SMX \rightarrow Fe^{III}(OH)_3 + P_1$ (12b)	(0.84 ± 0.24) M^{-1} s^{-1}	estimated in the Fe(VI)−CRE−micropollutant system
$Fe^{VI}O_4^{2-} + DAMP \rightarrow Fe^{III}(OH)_3 + P_1$ (12c)	(1.3 ± 0.3) M^{-1} s^{-1}	estimated in the Fe(VI)−CRE−micropollutant system
$Fe^{VI}O_4^{2-} + CBZ \rightarrow Fe^{III}(OH)_3 + P_1$ (12d)	(1.3 ± 0.3) M^{-1} s^{-1}	estimated in the Fe(VI)−CRE−micropollutant system
$Fe^{VI}O_4^{2-} + AMI \rightarrow Fe^{III}(OH)_3 + P_1$ (12e)	(1.3 ± 0.1) M^{-1} s^{-1}	estimated in the Fe(VI)−CRE−micropollutant system
$Fe^{IV}O_3^{2-} + TMP \rightarrow Fe^{III}(OH)_3 + P_2$ (13a)	(8.3 ± 0.6) × 10^4 M^{-1} s^{-1}	estimated in the Fe(VI)−CRE−micropollutant system
$Fe^{IV}O_3^{2-} + SMX \rightarrow Fe^{III}(OH)_3 + P_2$ (13b)	(7.9 ± 0.4) × 10^4 M^{-1} s^{-1}	estimated in the Fe(VI)−CRE−micropollutant system
$Fe^{IV}O_3^{2-} + DAMP \rightarrow Fe^{III}(OH)_3 + P_2$ (13c)	(4.5 ± 0.3) × 10^4 M^{-1} s^{-1}	estimated in the Fe(VI)−CRE−micropollutant system
$Fe^{IV}O_3^{2-} + CBZ \rightarrow Fe^{III}(OH)_3 + P_2$ (13d)	(3.5 ± 0.3) × 10^4 M^{-1} s^{-1}	estimated in the Fe(VI)−CRE−micropollutant system
$Fe^{IV}O_3^{2-} + AMI \rightarrow Fe^{III}(OH)_3 + P_2$ (13e)	(2.2 ± 0.1) × 10^4 M^{-1} s^{-1}	estimated in the Fe(VI)−CRE−micropollutant system

[a] $Fe^{IV}O_3^{2-}$ is the proposed chemical formula of Fe(IV) and Reactions 3−6 and 8 from the previous studies are modified in this study. [b] The contribution of $HFeO_4^-$ was not shown for simplicity as it only accounted for less than 2% of the concentration of Fe(VI) at pH 9.0. [c] eqs 11-13 were primarily balanced based iron species for simplicity. P_1 and P_2 refer to oxidation products of organics generally.

result also agreed with the prediction that amine-containing reductants are usually $R_{(2)}$ by previous literature.[51]

OPs of SMX by Fe(VI)−Micropollutant and Fe(VI)−CRE−Micropollutant Systems. There were no apparent differences in products distribution for the degradation of SMX by the Fe(VI)−micropollutant and Fe(VI)−CRE−micropollutant systems based on the identifiable products in this study. Cleavage of the S−N bond, oxidation of the aniline group, and hydroxylation of the benzene ring of SMX were found to be the main transformation pathways, which were consistent with previous studies.[10,52] More detailed information is described in SI Text S5. The similar products found in the Fe(VI)−micropollutant and Fe(VI)−CRE−micropollutant systems were also observed in ammonium-,[17] acid-,[53] bicarbonate-,[10] and sulfite[54] -activated Fe(VI) systems, indicating that these generated or complexed iron intermediate species (Fe(V)/Fe(IV)) can significantly alter the oxidation rate but not the types of main products.

Kinetic Investigation of Fe(VI)−CRE system (Eqs 1−11). *Kinetic Formulation.* As discussed above, Fe(IV) is considered as the major reactive species contributing to the enhanced degradation rate of pharmaceuticals in the presence of CRE. A total of 11 reactions (eqs 1−10 in Table 1) are proposed to represent the Fe(VI) decay at pH 9.0 involving high-valent iron intermediate species in phosphate-buffered aqueous systems, based on our previous study.[55] eq 1 represents the initiation of Fe(VI) decay in which unimolecular Fe(VI) decay occurs to produce one Fe(IV) and one H_2O_2. The newly formed Fe(IV) species can undergo dimerization to form di-Fe(IV) (eq 3), which further self-decomposes to Fe(III) and H_2O_2 (eq 4). The formed mono-Fe(IV) can also react with H_2O_2 to produce Fe(II) and O_2 (eq 5) via a concerted two-electron transfer pathway. On the other hand, Fe(IV) and Fe(VI) can also react with the newly generated Fe(II) from eq 5 to yield Fe(V) and Fe(III) (eqs 6 and 7). Fe(V) can undergo self-decomposition via first (eq 9a) and second (eq 9b) order decays, as well as reaction with H_2O_2 (eq 10). eq 2 represents Fe(VI) oxidation of H_2O_2 via two-electron transfer to generate Fe(IV) and O_2. However, $k_2 = 0$ M^{-1} s^{-1} was assigned to this reaction based on the model simulation of H_2O_2 generation at pH 9.0[55] and the kinetic investigation between FeO_4^{2-} and H_2O_2.[56] The later study

https://dx.doi.org/10.1021/acsestwater.0c00255
ACS EST Water 2021, 1, 969−979

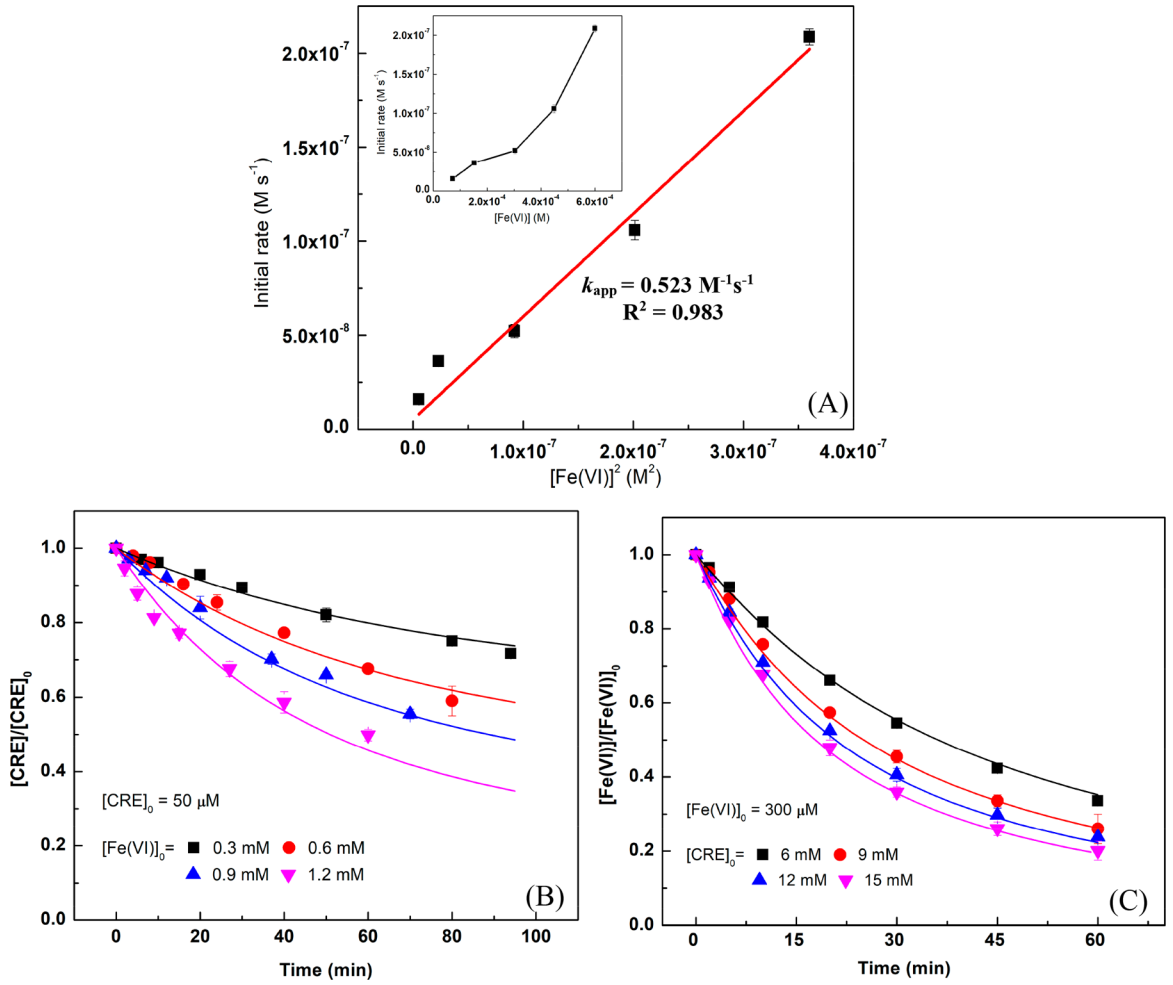

Figure 3. (A) Relationship between the initial Fe(VI) decay rate and initial $[Fe(VI)]^2$ in the presence of excess CRE; Inset shows the corresponding plot of initial rate vs [Fe(VI)]. Initially, [CRE] = 5.0 mM and [Fe(VI)] = 72.0−600.0 μM. (B,C) Measured and predicted (eqs 1−11) degradation of CRE and Fe(VI) in the Fe(VI)−CRE system. Symbols: measured data; Lines: model calculation; Error bars: one standard deviation of data. All reactions were at pH 9.0 (10.0 mM phosphate buffer), 25.0 °C, and n = 2.

pointed out that the oxidation of H_2O_2 requires prior coordination of peroxide to the metal to initiate inner-sphere electron transfer, but FeO_4^{2-}, owing to a slower oxygen exchange rate[57] compared to that of its protonated counterparts (i.e., $HFeO_4^-$, H_2FeO_4, and $H_3FeO_4^+$), could not achieve such ligand substitution, let alone the electron transfer process afterward.[56]

Interaction between Fe(VI) and CRE. Because CRE is known to be a ligand for various metal ions (e.g., Cu(II),[29] Ni(II),[58] Ag(I),[58] Zn(II),[59] Pt(II),[59] and Fe(III)[30]), CRE might be hypothesized to complex with Fe(VI)/Fe(IV). We explored the formation of Fe(VI)−CRE complex and/or Fe(IV)−CRE complex during the oxidation of CRE by Fe(VI) by performing stopped-flow spectroscopic kinetic studies. Results at different reaction time periods from 0 to 10 ms to 0−1000 s are shown in SI Figure S5. Spectra (SI Figure S5) collected in our study had no observable shift of Fe(VI) spectra at 510 nm, with only observable decay of Fe(VI) when the reaction time was longer. Also, no growth of a new spectrum at 410 nm could be observed, which corresponds to the characteristic peak of Fe(IV) species in aqueous solution.[60,61] Current literature[62−64] indicate that the Fe(IV) complexes with nitrogen-containing ligands can only be observed in a nonaqueous environment at low temperature (<−20 °C) that require bulky organic ligands. Our results suggested that the Fe(VI)−CRE complex was not inclined to form and the Fe(IV)−CRE complex was unlikely to be observed experimentally in an alkaline aqueous environment (i.e., pH 9.0 PBS).

CRE, on the other hand, is a reactant in the Fe(VI)−CRE system. Under the pseudo-first-order reaction condition where $[Fe(VI)]_0$ was 6−30 times of $[CRE]_0$, the observed first-order rate constant of CRE degradation remained consistent at (3.6 ± 0.3) × 10^{-3} min^{-1} as $[CRE]_0$ was increased from 10.0 to 50.0 μM (SI Figure S6). This result verified that the reaction between Fe(VI) and CRE is first-order with respect to CRE. When experiments were conducted under the pseudo-first-order reaction condition where $[CRE]_0$ was 8.3−70 times of $[Fe(VI)]_0$, the observed first-order rate constant of Fe(VI) decay decreased from 3.8 × 10^{-2} to 1.8 × 10^{-2} min^{-1} when $[Fe(VI)]_0$ was increased from 72.0 to 600.0 μM (SI Figure S7). This result indicated that the reaction between Fe(VI) and CRE is not first-order with respect to Fe(VI). The method of initial rate was used to determine the reaction order of Fe(VI) degradation in the Fe(VI)−CRE system (SI Text S6). As shown in Figure 3A, a linear relationship could only be established between the initial Fe(VI) decay rate and $[Fe(VI)]^2$ while no linearity was seen between the initial rate

https://dx.doi.org/10.1021/acsestwater.0c00255
ACS EST Water 2021, 1, 969−979

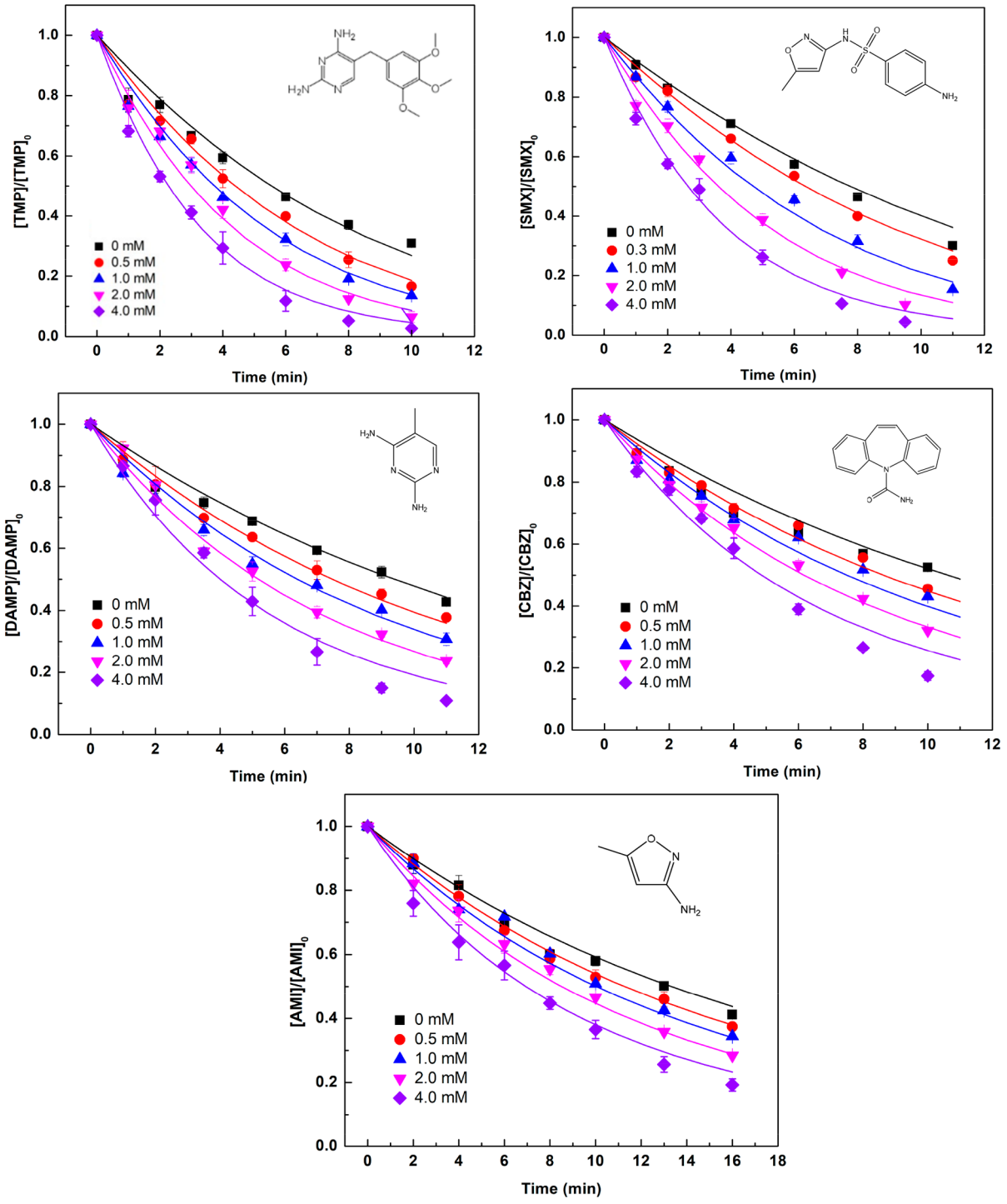

Figure 4. Measured and predicted (eqs 1−13) degradation of micropollutants by the Fe(VI)−CRE−micropollutant system. Symbols: measured data; lines: model calculation; Error bars: one standard deviation of data. Initially, [micropollutant] = 10.0 μM, [Fe(VI)] = 300.0 μM, [CRE] = 0−4.0 mM. Reactions were at pH 9.0 (10.0 mM phosphate buffer), 25.0 °C, and n = 2.

and [Fe(VI)], suggesting the reaction could be second-order with respect to Fe(VI). The above kinetic experimental results are consistent with the rate law of $v = k_{11}[\text{CRE}][\text{FeO}_4^{2-}]^2 = k_{app}[\text{FeO}_4^{2-}]^2$, where k_{app} = 0.523 M^{-1} s^{-1} and k_{11} = 104.5 M^{-2} s^{-1} at pH 9.0.

A plausible explanation is that CRE (present in much excess to Fe(VI)) in the Fe(VI)−CRE system may serve as a bridge to interconnect with two mono FeO_4^{2-} to facilitate the bimolecular reaction of Fe(VI), in contrast to the unimolecular decay of Fe(VI) in Fe(VI)-only system at pH 9.0 as identified by our previous study.[55] A similar phenomenon was also proposed by Ma and co-workers,[65] in which an accelerating effect of Ca^{2+} on Fe(VI) decay at pH 9.0−10.0 was observed to initiate the dimerization of FeO_4^{2-} species with the help of metal cations such as Ca^{2+} to bridge two FeO_4^{2-} ions.

Model Validation. On the basis of the above results, eq 11 was added to the kinetic model of the Fe(VI)−CRE system to represent the third-order reaction between Fe(VI) and CRE,

https://dx.doi.org/10.1021/acsestwater.0c00255
ACS EST Water 2021, 1, 969−979

where k_{11} = 104.5 M^{-2} s^{-1} was derived experimentally according to Figure 3**A.** Then, additional experiments under varying reaction conditions were employed to further validate the proposed eq 11.

In Figure 3B,C, model simulations of Fe(VI) and CRE evolution were conducted for various reaction conditions of $[CRE]_0$ and $[Fe(VI)]_0$ and compared with the experimental data. According to the statistical analysis of the experimental and simulated removal efficiency (in %) (SI Figure S8) and goodness-of-fit (SI Text S7 and Table S4), the simulated Fe(VI) and CRE decay profiles agreed well with the experimental data with TIC = 0.01−0.02, ME = 0.998−0.999, and NRMSE = 2.58 × 10^{-2}−5.70 × 10^{-2}, which validated the proposed eq 11 in the Fe(VI)−CRE system.

Kinetic Investigation of Fe(IV)−CRE−Micropollutant System (Eqs 1−13). *Kinetic Formulation.* Based on the Fe(VI)−CRE system, two sets of eqs 12 and 13 were added for the Fe(VI)−CRE−micropollutant system to represent the most important interaction between high-valent iron species and micropollutant. eqs 12a−12e represent the reactions between Fe(VI) and micropollutants, whereas eqs 13a−13e represent the reactions between Fe(IV) and micropollutants. Fe(IV) was confirmed to be the major intermediate reactive iron species based on PMSO oxidation experiments and DFT calculations as discussed above. Moreover, the simulated Fe(IV) and Fe(V) evolution profiles in the Fe(VI)−CRE system (SI Figure S9) showed that Fe(V) was at least two-orders of magnitude lower in concentration compared to Fe(IV) when CRE concentration was lower than 4.0 mM. This again supports that Fe(V) is a less important oxidant to promote the degradation of micropollutants in Fe(VI)−CRE−micropollutant system, unless Fe(V) reactivity toward the micropollutant is at least 2 orders of magnitude higher than its Fe(IV) counterpart. Currently, the reactivity trend of Fe(V) and Fe(IV) in alkaline condition is scarce in the literature, and is limited to cyanide at pH ≥ 10.5 only.[42,66]

Model Validation. By adopting the Fe(VI)−CRE−micropollutant system including eqs 1−13, the kinetic model was applied to simulate the experimental data of degradation of micropollutants at different CRE concentrations to derive k_{12} and k_{13} values (Figure 4 and Table 1). According to the statistical analysis of the experimental and simulated removal efficiency (SI Figure S10) and goodness-of-fit (SI Text S7 and Table S5), the simulated micropollutant degradation profiles agreed well with the experimental degradation profiles of the five compounds within the first 15 min with TIC = 0.01−0.06, ME = 0.995−0.999, and NRMSE = 2.91 × 10^{-2}−4.61 × 10^{-2}, which validated the proposed eqs 12 and 13 in the Fe(VI)−CRE−micropollutant system. This kinetic model can accurately predict not only the micropollutant degradation but also the Fe(VI) and CRE decays as shown in Figure 5, both of which assisted to improve the robustness of the model. Moreover, the simulated k_{12} values ranged at 2.2 × 10^4 to 8.3 × 10^4 M^{-1} s^{-1}, which agreed well with other Fe(IV) oxidation studies with aromatic compounds that reported the rate constant range at 1.05 × 10^3−1.5 × 10^4 M^{-1} s^{-1} at pH 0−3.[67]

It should be noted that the proposed kinetic model started to deviate from the observed degradation trends for DAMP and CBZ at 4.0 mM CRE after 6.0 min, which could be explained by possible involvement Fe(V) at higher CRE concentration conditions. Simulations for the Fe(VI)−CRE system indicate that the molar ratio of Fe(IV)/Fe(V) starts to decrease to be below 100 at 2.5 min as $[CRE]_0$ is increased

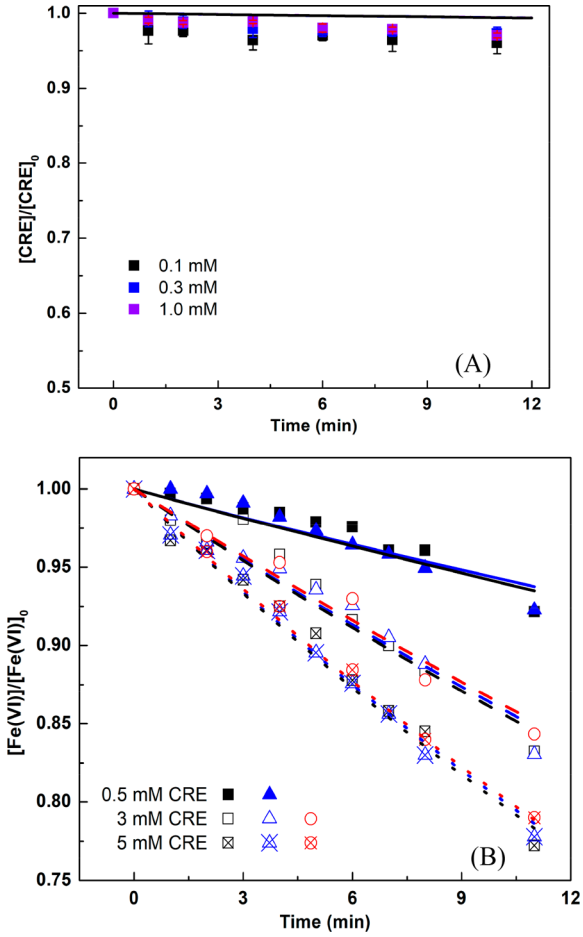

Figure 5. Measured and predicted decay of (A) CRE and (B) Fe(VI) in the Fe(VI)−CRE−micropollutant system. Symbols: measured data; lines: model calculation; error bars: one standard deviation of data. Experimental conditions: (A) [SMX] = 10.0 μM, [Fe(VI)] = 300.0 μM, [CRE] = 0.1−1.0 mM; (B) [micropollutant] = 10.0 μM, [Fe(VI)] = 300.0 μM, [CRE] = 0.5, 3.0, and 5.0 mM. In (A), the simulation results overlapped. In (B), symbols are square (TMP), triangle (CBZ), and circle (SMX); lines are black (TMP), blue (CBZ), and red (SMX). All reactions were at pH 9.0 (10.0 mM phosphate buffer) and 25 °C, n = 2.

above 4.0 mM (SI Figure S9C), while Fe(V) generated in situ begins to plateau and reach its peak around 6.0 min (SI Figure S8B). These two observations suggest that Fe(V) is able to emerge to play an increased role in interacting with the micropollutant at a high CRE concentration (≥4.0 mM) in the later stage (≥6.0 min), which could explain the underestimation of DAMP and CBZ degradation if Fe(V) happened to have a higher oxidative reactivity toward them compared to the rest of three compounds. Moreover, this can also help explain the peak k_{obs} occurred similarly at around 4.0 mM CRE for all three different pharmaceuticals in Figure 1B. This trend of decreased k_{obs} cannot be explained by simple competition of CRE with micropollutants for reactive Fe(IV) since the competition effect should have occurred at a lower CRE concentration for less reactive micropollutants (e.g., AMI and CBZ). Based on SI Figure S9C (simulations of Fe(IV)−CRE system), the significant decrease in the molar ratio of Fe(IV)/Fe(V) to below 100 after 2.5 min at CRE > 4.0 mM may promote the Fe(V)-driven oxidation and weaken Fe(IV) involvement. Moreover, CRE and/or its oxidization products

https://dx.doi.org/10.1021/acsestwater.0c00255
ACS EST Water 2021, 1, 969−979

may be further reacted in this highly oxidative environment with an elevated Fe(V)/Fe(IV) level, which could somehow inhibit the removal of target micropollutants. More research should be conducted to uncover the enhanced effects for Fe(V) and Fe(IV) at a high CRE dosage (i.e., > 4.0 mM) and to differentiate the individual contributions of these two high-valent iron species.

CONCLUSIONS

The extensive occurrence of pharmaceuticals in the aquatic environment and potable water demands more efficient treatment of these micropollutants from the urine source. Fe(VI) application to chemically remove such micropollutants in hydrolyzed urine could stand out because of its resistance to the scavenging effects of urine matrix and advantageous enhancement effects from several major urine constituents such as bicarbonate,[10] ammonia,[10,17] and CRE. This paper, for the first time, reports the enhancement of Fe(VI) oxidation by CRE and quantitatively explains the enhancement effect by the generation of high-valent iron intermediate species (i.e., Fe(IV)) using a comprehensive Fe(VI)−CRE−micropollutant model. Based on this kinetic model, the rate constants between micropollutants and Fe(IV) can be derived (within CRE concentration of 0−4.0 mM and at pH 9.0). This approach can be conceptually useful to probe the kinetic behaviors of iron intermediate species in the Fe(VI)−reductant system. This model may be further used to evaluate the reactivity of Fe(IV) toward more micropollutants with distinctive function groups, and serve as the bridge for mechanistic investigation and optimization of application of Fe(VI) oxidation. In addition, future research should evaluate the effects of other urine constituents (e.g., other organics or partially degraded organic matter) on the Fe(VI) oxidation reaction, optimization of Fe(VI) oxidation of pharmaceuticals in real urine, as well as how the pharmaceutical degradation can be effectively combined with other treatment (i.e., nutrients recovery) of urine holistically.

ASSOCIATED CONTENT

Supporting Information

The Supporting Information is available free of charge at https://pubs.acs.org/doi/10.1021/acsestwater.0c00255.

Text S1, information on urine organic metabolites; Texts S2−S4, information on chemicals and experimental and calculationprocedures; Text S5, products analysis by Fe(VI)−SMX and Fe(VI)−CRE−SMX systems; Text S6, measurement of initial decay rate; Text S7, goodness-of-fit of the kinetic model; Table S1, chemical properties of structures of compounds investigated in this study; Table S2, hydrolyzed urine recipe; Table S3, analysis data of SMX and its OPs; Table S4, goodness-of-fit of Figure 3B,C based on TIC; Table S5, goodness-of-fit of Figure 4 based on TIC; Figure S1, Fe(VI) oxidation of TMT, DMI, and aniline; Figure S2, LT-EPR spectra of Fe(VI) oxidation of CRE; Figure S3, DFT calculations of Gibbs free energy of one-electron vs two-electron transfer pathways for the initial reaction between Fe(VI) and CRE; Figure S4, mass spectra of SMX and its OPs; Scheme S1, proposed reaction pathways of SMX degradation by Fe(VI)-SMX and Fe(VI)−CRE−SMX systems; Figure S5, stopped-flow UV−vis spectra of Fe(VI) and CRE in pH 9.0 (10.0 mM phosphate buffer); Figure S6, relative logarithmic concentration of CRE as a function of reaction time during Fe(VI) oxidation of CRE at pH 9.0; Figure S7, relative logarithmic concentration of Fe(VI) as a function of reaction time during Fe(VI) oxidation of CRE at pH 9.0; Figure S8, statistic analysis of goodness-of-fit between simulation of experimental results in Fe(VI)−CRE system; Figure S9, simulated Fe(V)/Fe(IV) evolution profile in Fe(VI)−CRE system; Figure S10, statistic analysis of goodness-of-fit between simulation of experimental results in simplified Fe(VI)−CRE−micropollutant system (PDF)

AUTHOR INFORMATION

Corresponding Authors

Virender K. Sharma − *Department of Environment and Occupational Health, School of Public Health, Texas A&M University, College Station, Texas 77843, United States;* orcid.org/0000-0002-5980-8675; Email: vsharma@tamu.edu

Ching-Hua Huang − *School of Civil and Environmental Engineering, Georgia Institute of Technology, Atlanta, Georgia 30332, United States;* orcid.org/0000-0002-3786-094X; Email: ching-hua.huang@ce.gatech.edu

Authors

Cong Luo − *School of Civil and Environmental Engineering, Georgia Institute of Technology, Atlanta, Georgia 30332, United States*

Mingbao Feng − *Department of Environment and Occupational Health, School of Public Health, Texas A&M University, College Station, Texas 77843, United States*

Tianqi Zhang − *School of Civil and Environmental Engineering, Georgia Institute of Technology, Atlanta, Georgia 30332, United States;* orcid.org/0000-0001-6577-315X

Complete contact information is available at: https://pubs.acs.org/10.1021/acsestwater.0c00255

Notes

The authors declare no competing financial interest.

ACKNOWLEDGMENTS

This work was supported by the projects from National Science Foundation (CBET 1802944 and CBET 1802800). Any opinions, findings, and conclusions or recommendations expressed in this material are those of the authors and do not necessarily reflect the views of the National Science Foundation.

REFERENCES

(1) Maurer, M.; Schwegler, P.; Larsen, T. Nutrients in urine: energetic aspects of removal and recovery. *Water Sci. Technol.* **2003**, *48* (1), 37−46.

(2) Lienert, J.; Bürki, T.; Escher, B. I. Reducing micropollutants with source control: substance flow analysis of 212 pharmaceuticals in faeces and urine. *Water Sci. Technol.* **2007**, *56* (5), 87−96.

(3) Pronk, W.; Palmquist, H.; Biebow, M.; Boller, M. Nanofiltration for the separation of pharmaceuticals from nutrients in source-separated urine. *Water Res.* **2006**, *40* (7), 1405−1412.

(4) Landry, K. A.; Sun, P.; Huang, C.-H.; Boyer, T. H. Ion-exchange selectivity of diclofenac, ibuprofen, ketoprofen, and naproxen in ureolyzed human urine. *Water Res.* **2015**, *68*, 510−521.

(5) Tarpeh, W. A.; Barazesh, J. M.; Cath, T. Y.; Nelson, K. L. Electrochemical stripping to recover nitrogen from source-separated urine. *Environ. Sci. Technol.* **2018**, *52* (3), 1453−1460.
(6) Kemacheevakul, P.; Chuangchote, S.; Otani, S.; Matsuda, T.; Shimizu, Y. Phosphorus recovery: Minimization of amount of pharmaceuticals and improvement of purity in struvite recovered from hydrolyzed urine. *Environ. Technol.* **2014**, *35* (23), 3011−3019.
(7) Solanki, A.; Boyer, T. H. Pharmaceutical removal in synthetic human urine using biochar. *Environ. Sci. Water Res. Technol.* **2017**, *3* (3), 553−565.
(8) Dodd, M. C.; Zuleeg, S.; von Gunten, U.; Pronk, W. Ozonation of source-separated urine for resource recovery and waste minimization: Process modeling, reaction chemistry, and operational considerations. *Environ. Sci. Technol.* **2008**, *42* (24), 9329−9337.
(9) Zhang, R.; Yang, Y.; Huang, C.-H.; Li, N.; Liu, H.; Zhao, L.; Sun, P. UV/H_2O_2 and UV/PDS treatment of trimethoprim and sulfamethoxazole in synthetic human urine: Transformation products and toxicity. *Environ. Sci. Technol.* **2016**, *50* (5), 2573−2583.
(10) Luo, C.; Feng, M.; Sharma, V. K.; Huang, C.-H. Oxidation of pharmaceuticals by ferrate(VI) in hydrolyzed urine: Effects of major inorganic constituents. *Environ. Sci. Technol.* **2019**, *53* (9), 5272−5281.
(11) Bouatra, S.; Aziat, F.; Mandal, R.; Guo, A. C.; Wilson, M. R.; Knox, C.; Bjorndahl, T. C.; Krishnamurthy, R.; Saleem, F.; Liu, P.; Dame, Z. T.; Poelzer, J.; Huynh, J.; Yallou, F. S.; Psychogios, N.; Dong, E.; Bogumil, R.; Roehring, C.; Wishart, D. S. The Human Urine Metabolome. *PLoS One* **2013**, *8* (9), e73076.
(12) Udert, K. M.; Larsen, T. A.; Gujer, W. Fate of major compounds in source-separated urine. *Water Sci. Technol.* **2006**, *54* (11−12), 413−420.
(13) Putnam, D. F., Composition and concentrative properties of human urine. 1971, NASA contrator report, document ID 19710023044, https://ntrs.nasa.gov/citations/19710023044.
(14) Sykes, B. D. Urine stability for metabolomic studies: Effects of preparation and storage. *Metabolomics* **2007**, *3* (1), 19−27.
(15) Sharma, V. K.; Anquandah, G. A.; Nesnas, N. Kinetics of the oxidation of endocrine disruptor nonylphenol by ferrate(VI). *Environ. Chem. Lett.* **2009**, *7* (2), 115−119.
(16) Lee, Y.; Zimmermann, S. G.; Kieu, A. T.; von Gunten, U. Ferrate (Fe(VI)) application for municipal wastewater treatment: A novel process for simultaneous micropollutant oxidation and phosphate removal. *Environ. Sci. Technol.* **2009**, *43*, 3831−3838.
(17) Feng, M.; Cizmas, L.; Wang, Z.; Sharma, V. K. Activation of ferrate(VI) by ammonia in oxidation of flumequine: Kinetics, transformation products, and antibacterial activity assessment. *Chem. Eng. J.* **2017**, *323*, 584−591.
(18) Manoli, K.; Nakhla, G.; Ray, A. K.; Sharma, V. K. Enhanced oxidative transformation of organic contaminants by activation of ferrate(VI): Possible involvement of Fe^{V}/Fe^{IV} species. *Chem. Eng. J.* **2017**, *307*, 513−517.
(19) Shao, B.; Dong, H.; Sun, B.; Guan, X. Role of ferrate(IV) and ferrate(V) in activating ferrate(VI) by calcium sulfite for enhanced oxidation of organic contaminants. *Environ. Sci. Technol.* **2019**, *53* (2), 894−902.
(20) Zhao, J.; Liu, Y.; Wang, Q.; Fu, Y.; Lu, X.; Bai, X. The self-catalysis of ferrate(VI) by its reactive byproducts or reductive substances for the degradation of diclofenac: Kinetics, mechanism and transformation products. *Sep. Purif. Technol.* **2018**, *192*, 412−418.
(21) Zhao, J.; Wang, Q.; Fu, Y.; Peng, B.; Zhou, G. Kinetics and mechanism of diclofenac removal using ferrate(VI): Roles of Fe^{3+}, Fe^{2+}, and Mn^{2+}. *Environ. Sci. Pollut. Res.* **2018**, *25* (23), 22998−23008.
(22) Hughes, S. R.; Kay, P.; Brown, L. E. Global synthesis and critical evaluation of pharmaceutical data sets collected from river systems. *Environ. Sci. Technol.* **2013**, *47* (2), 661−677.
(23) Zhang, T.; Li, B. Occurrence, transformation, and fate of antibiotics in municipal wastewater treatment plants. *Crit. Rev. Environ. Sci. Technol.* **2011**, *41* (11), 951−998.
(24) Yang, C.; Liu, H.; Li, M.; Yu, C. Treating urine by *Spirulina platensis*. *Acta Astronaut.* **2008**, *63* (7), 1049−1054.
(25) Zhang, R.; Sun, P.; Boyer, T. H.; Zhao, L.; Huang, C. H. Degradation of pharmaceuticals and metabolite in synthetic human urine by UV, UV/H_2O_2, and UV/PDS. *Environ. Sci. Technol.* **2015**, *49* (5), 3056−66.
(26) Theil, H. *Economic Forecasts and Policy*; North-Holland Publishing Company: Amsterdam, 1961.
(27) Esposito, G.; Frunzo, L.; Panico, A.; Pirozzi, F. Model calibration and validation for OFMSW and sewage sludge co-digestion reactors. *Waste Manage.* **2011**, *31* (12), 2527−2535.
(28) Anquandah, G. A.; Sharma, V. K.; Knight, D. A.; Batchu, S. R.; Gardinali, P. R. Oxidation of trimethoprim by ferrate(VI): Kinetics, products, and antibacterial activity. *Environ. Sci. Technol.* **2011**, *45* (24), 10575−81.
(29) Chan, P. C.; Kesner, L. Copper (II) complex-catalyzed oxidation of NADH by hydrogen peroxide. *Biol. Trace Elem. Res.* **1980**, *2* (3), 159−174.
(30) Pugia, M. J.; Lott, J. A.; Wallace, J. F.; Cast, T. K.; Bierbaum, L. D. Assay of creatinine using the peroxidase activity of copper-creatinine complexes. *Clin. Biochem.* **2000**, *33* (1), 63−70.
(31) Singh, A.; Patra, S.; Lee, J.-A.; Park, K. H.; Yang, H. An artificial enzyme-based assay: DNA detection using a peroxidase-like copper−creatinine complex. *Biosens. Bioelectron.* **2011**, *26* (12), 4798−4803.
(32) Nagaraja, P.; Avinash, K.; Shivakumar, A.; Krishna, H. Quantification of creatinine in biological samples based on the pseudoenzyme activity of copper−creatinine complex. *Spectrochim. Acta, Part A* **2012**, *92*, 318−324.
(33) Chen, G.; Lam, W. W.; Lo, P.-K.; Man, W.-L.; Chen, L.-J.; Lau, K.-C.; Lau, T.-C. Mechanism of water oxidation by ferrate(VI) at pH 7−9. *Chem. - Eur. J.* **2018**, *24* (70), 18735−18742.
(34) Huang, Z.-S.; Wang, L.; Liu, Y.-L.; Jiang, J.; Xue, M.; Xu, C.-B.; Zhen, Y.-F.; Wang, Y.-C.; Ma, J. Impact of phosphate on ferrate oxidation of organic compounds: An underestimated oxidant. *Environ. Sci. Technol.* **2018**, *52* (23), 13897−13907.
(35) Dong, H.; Li, Y.; Wang, S.; Liu, W.; Zhou, G.; Xie, Y.; Guan, X. Both Fe(IV) and radicals are active oxidants in the Fe(II)/peroxydisulfate process. *Environ. Sci. Technol. Lett.* **2020**, *7* (3), 219−224.
(36) Elovitz, M. S.; von Gunten, U. Hydroxyl radical/ozone ratios during ozonation processes. I. The R_{ct} concept. *Ozone: Sci. Eng.* **1999**, *21*, 239−260.
(37) Pestovsky, O.; Bakac, A. Aqueous ferryl(IV) ion: Kinetics of oxygen atom transfer to substrates and oxo exchange with solvent water. *Inorg. Chem.* **2006**, *45* (2), 814−820.
(38) Bataineh, H.; Pestovsky, O.; Bakac, A. pH-Induced mechanistic changeover from hydroxyl radicals to iron(IV) in the Fenton reaction. *Chem. Sci.* **2012**, *3* (5), 1594−1599.
(39) Chen, J.; Xu, X.; Zeng, X.; Feng, M.; Qu, R.; Wang, Z.; Nesnas, N.; Sharma, V. K. Ferrate(VI) oxidation of polychlorinated diphenyl sulfides: Kinetics, degradation, and oxidized products. *Water Res.* **2018**, *143*, 1−9.
(40) Li, H.; Shan, C.; Pan, B. Fe(III)-doped g-C_3N_4 mediated peroxymonosulfate activation for selective degradation of phenolic compounds via high-valent iron-oxo species. *Environ. Sci. Technol.* **2018**, *52* (4), 2197−2205.
(41) Pang, S.-Y.; Jiang, J.; Ma, J. Oxidation of sulfoxides and arsenic(III) in corrosion of nanoscale zero valent iron by oxygen: evidence against ferryl ions (Fe(IV)) as active intermediates in Fenton reaction. *Environ. Sci. Technol.* **2011**, *45* (1), 307−312.
(42) Sharma, V. K. Ferrate(VI) and ferrate(V) oxidation of organic compounds: Kinetics and mechanism. *Coord. Chem. Rev.* **2013**, *257* (2), 495−510.
(43) Kralchevska, R. P.; Sharma, V. K.; Machala, L.; Zboril, R. Ferrates(Fe(VI), Fe(V), and Fe(IV)) oxidation of iodide: Formation of triiodide. *Chemosphere* **2016**, *144*, 1156−61.
(44) Sharma, V. K.; Luther, G. W.; Millero, F. J. Mechanisms of oxidation of organosulfur compounds by ferrate(VI). *Chemosphere* **2011**, *82* (8), 1083−1089.

https://dx.doi.org/10.1021/acsestwater.0c00255
ACS EST Water 2021, 1, 969−979

(45) Anquandah, G. A.; Sharma, V. K.; Panditi, V. R.; Gardinali, P. R.; Kim, H.; Oturan, M. A. Ferrate (VI) oxidation of propranolol: Kinetics and products. *Chemosphere* **2013**, *91* (1), 105−109.
(46) Sharma, V. K. Oxidation of inorganic contaminants by ferrates(VI, V, and IV) − kinetics and mechanisms: A review. *J. Environ. Manage.* **2011**, *92* (4), 1051−1073.
(47) Sharma, V. K. Oxidation of inorganic compounds by ferrate(VI) and ferrate(V): One-electron and two-electron transfer steps. *Environ. Sci. Technol.* **2010**, *44* (13), 5148−5152.
(48) Terryn, R. J., III; Huerta-Aguilar, C. A.; Baum, J. C.; Sharma, V. K. Fe^{VI}, Fe^{V}, and Fe^{IV} oxidation of cyanide: Elucidating the mechanism using density functional theory calculations. *Chem. Eng. J.* **2017**, *330*, 1272−1278.
(49) Inoue, S.; Kawanishi, S. ESR evidence for superoxide, hydroxyl radicals and singlet oxygen produced from hydrogen peroxide and nickel(II) complex of glycylglycyl-L-histidine. *Biochem. Biophys. Res. Commun.* **1989**, *159* (2), 445−451.
(50) Huang, H.; Sommerfeld, D.; Dunn, B. C.; Lloyd, C. R.; Eyring, E. M. Ferrate(VI) oxidation of aniline. *J. Chem. Soc., Dalton. Trans.* **2001**, 1301−1305.
(51) Feng, M.; Jinadatha, C.; McDonald, T. J.; Sharma, V. K. Accelerated oxidation of organic contaminants by ferrate(VI): The overlooked role of reducing additives. *Environ. Sci. Technol.* **2018**, *52* (19), 11319−11327.
(52) Sharma, V. K.; Mishra, S. K.; Nesnas, N. Oxidation of sulfonamide antimicrobials by ferrate(VI)[$Fe^{VI}O_4^{2-}$]. *Environ. Sci. Technol.* **2006**, *40* (23), 7222−7227.
(53) Manoli, K.; Nakhla, G.; Ray, A. K.; Sharma, V. K. Oxidation of caffeine by acid-activated ferrate(VI): Effect of ions and natural organic matter. *AIChE J.* **2017**, *63* (11), 4998−5006.
(54) Feng, M.; Sharma, V. K. Enhanced oxidation of antibiotics by ferrate(VI)-sulfur(IV) system: Elucidating multi-oxidant mechanism. *Chem. Eng. J.* **2018**, *341*, 137−145.
(55) Luo, C.; Feng, M.; Sharma, V. K.; Huang, C.-H. Revelation of ferrate(VI) unimolecular decay under alkaline conditions: Investigation of involvement of Fe(IV) and Fe(V) species. *Chem. Eng. J.* **2020**, *388*, 124134.
(56) Rush, J. D.; Zhao, Z.; Bielski, B. H. Reaction of ferrate(VI)/ferrate(V) with hydrogen peroxide and superoxide anion - A stopped-flow and premix pulse radiolysis study. *Free Radical Res.* **1996**, *24* (3), 187−198.
(57) Goff, H.; Murmann, R. K. Mechanism of isotopic oxygen exchange and reduction of ferrate(VI) ion (FeO_4^{2-}). *J. Am. Chem. Soc.* **1971**, *93* (23), 6058−6065.
(58) Mitewa, M.; Gencheva, G.; Bontchev, P. R.; Zhecheva, E.; Nefedov, V. Structure of Ni(II)-creatinine complex species formed in non-aqueous media. *Inorg. Chim. Acta* **1989**, *164* (2), 201−204.
(59) Muralidharan, S.; Nagaraja, K.; Udupa, M. Creatinine complexes of zinc, cadmium and mercury. *Polyhedron* **1984**, *3* (5), 619−621.
(60) Bielski, B. H. [4] Generation of iron(IV) and iron(V) complexes in aqueous solutions. *Methods Enzymol.* **1990**, *186*, 108−113.
(61) Melton, J. D.; Bielski, B. H. Studies of the kinetic, spectral and chemical properties of Fe(IV) pyrophosphate by pulse radiolysis. *Int. J. Radiat. Appl. Instrum. C. Radiat. Phys. Chem.* **1990**, *36* (6), 725−733.
(62) Lu, X.; Li, X.-X.; Seo, M. S.; Lee, Y.-M.; Clémancey, M.; Maldivi, P.; Latour, J.-M.; Sarangi, R.; Fukuzumi, S.; Nam, W. A mononuclear nonheme iron(IV)−amido complex relevant for the compound II chemistry of cytochrome P450. *J. Am. Chem. Soc.* **2019**, *141* (1), 80−83.
(63) Dantignana, V.; Serrano-Plana, J.; Draksharapu, A.; Magallón, C.; Banerjee, S.; Fan, R.; Gamba, I.; Guo, Y.; Que, L., Jr; Costas, M. Spectroscopic and reactivity comparisons between nonheme oxoiron(IV) and oxoiron(V) species bearing the same ancillary ligand. *J. Am. Chem. Soc.* **2019**, *141* (38), 15078−15091.
(64) Lu, X.; Li, X.-X.; Lee, Y.-M.; Jang, Y.; Seo, M. S.; Hong, S.; Cho, K.-B.; Fukuzumi, S.; Nam, W. Electron-transfer and redox reactivity of high-valent iron imido and oxo complexes with the formal oxidation states of five and six. *J. Am. Chem. Soc.* **2020**, *142* (8), 3891−3904.
(65) Ma, L.; Lam, W. W.; Lo, P. K.; Lau, K. C.; Lau, T. C. Ca^{2+}-induced oxidation generation by FeO_4^{2-} at pH 9−10. *Angew. Chem.* **2016**, *128* (9), 3064−3068.
(66) Sharma, V. K.; O'Connor, D. B.; Cabelli, D. E. Sequential one-electron reduction of Fe(V) to Fe(III) by cyanide in alkaline medium. *J. Phys. Chem. B* **2001**, *105* (46), 11529−11532.
(67) Mártire, D. O.; Caregnato, P.; Furlong, J.; Allegretti, P.; Gonzalez, M. C. Kinetic study of the reactions of oxoiron(IV) with aromatic substrates in aqueous solutions. *Int. J. Chem. Kinet.* **2002**, *34* (8), 488−494.
(68) Loegager, T.; Holcman, J.; Sehested, K.; Pedersen, T. Oxidation of ferrous ions by ozone in acidic solutions. *Inorg. Chem.* **1992**, *31* (17), 3523−3529.
(69) Lee, Y.; Kissner, R.; von Gunten, U. Reaction of ferrate(VI) with ABTS and self-decay of ferrate(VI): Kinetics and mechanisms. *Environ. Sci. Technol.* **2014**, *48* (9), 5154−5162.
(70) Sharma, V. K.; Bielski, B. H. Reactivity of ferrate(VI) and ferrate(V) with amino acids. *Inorg. Chem.* **1991**, *30* (23), 4306−4310.
(71) Pestovsky, O.; Bakac, A. Aqueous ferryl(IV) ion: Kinetics of oxygen atom transfer to substrates and oxo exchange with solvent water. *Inorg. Chem.* **2006**, *45* (2), 814−820.
(72) Rush, J. D.; Bielski, B. H. Decay of ferrate(V) in neutral and acidic solutions. A premix pulse radiolysis study. *Inorg. Chem.* **1994**, *33* (24), 5499−5502.
(73) Rush, J.; Bielski, B. H. Kinetics of ferrate(V) decay in aqueous solution. A pulse-radiolysis study. *Inorg. Chem.* **1989**, *28* (21), 3947−3951.

https://dx.doi.org/10.1021/acsestwater.0c00255
ACS EST Water 2021, 1, 969−979